Communications on Applied Nonlinear Analysis
ISSN: 1074-133X
Vol 31 No. 6s (2024)

Enhanced Lung Cancer Detection via Modified Fuzzy Analytic Hierarchy Process and FuzSquResMobileNet

A.Aruna[1], M.Vijaya [2]*,

[1] Research Scholar, Department of Mathematics, Marudupandiyar College,
Thanjavur, Tamil Nadu – 613403,

[2] Assistant Professor and Research Advisor, PG and Research Department of Mathematics,
Marudupandiyar college, Thanjavur, Tamil Nadu - 613403

Arunjo.jo21@gmail.com, mathvijaya23@gmail.com

(Affiliated to Bharathidasan University, Tiruchirappalli) * Corresponding Author

Article History:

Received: *16-06-2024*

Revised: *22-07-2024*

Accepted: *05-08-2024*

Abstract:

Lung cancer emphasizes the vital need of early detection in order to increase survival rates due to its high incidence of death worldwide. An effective methodology for lung cancer detection is proposed utilizing the Modified Fuzzy Analytic Hierarchy Process, a hybrid optimization algorithm. Gaussian filter and a modified Contrast Limited Adaptive Histogram Equalization (CLAHE) are employed for reliable pre-processing. This enhances the image quality and facilitates additional analysis. A novel hybrid ChimpGaz optimization that combines the optimizations of Gazelle and Chimp is employed to fine-tune the Mask R-CNN algorithm for Region of Interest (ROI) identification. This guarantees ideal parameter configurations for precise ROI division. A wide range of descriptors are used in feature extraction, such as shape features (area, circularity, and perimeter), geometric features (centroid, Euler number, and convexity), color features and texture features (Local Directional Patterns, or LDP, and Gabor Local Binary Patterns, or GLBP). These features are ranked using a Modified Fuzzy Analytic Hierarchy Process (AHP) that includes sigmoid membership functions customized for every feature. The hybrid optimization algorithm improves membership functions even more, strengthening the ranking system's capacity for discrimination. The proposed detection model, called "FuzSquResMobileNet," combines a sophisticated ensemble of pre-trained deep learning models (SqueezeNet, ResNet101, MobileNetv2) with fuzzy logic-based preliminary detection. Overall detection accuracy is improved by this fusion because it guarantees a thorough approach to feature extraction. Through incorporating fuzzy logic and deep learning, the methodology provides a promising avenue for effective and precise lung cancer detection, contributing to early intervention and improved patient outcomes.

Keywords: Lung cancer, CLAHE, Mask R-CNN, ChimpGaz optimization, Modified Fuzzy Analytic Hierarchy Process and Gabor Local Binary Patterns.

1. Introduction

In the world, lung cancer ranks among the top causes of death for both men and women, with a remarkable annual incidence rate of roughly five million fatal cases [1]. Since it manifests and manifests in its advanced stages, detection is challenging. Lung cancer ranked first for male deaths and third for female deaths in a database created by the International Agency for Research on Cancer (IARC) Global Cancer Observatory in 2018. The database included data on the prevalence and death

rates of 36 distinct cancer types in 185 countries [2]. It is the leading cause of cancer-related deaths globally, accounting for 1.6 million deaths annually. Advanced lung cancer patients still have a low 5-year survival rate (4% to 17%), despite the availability of multimodality treatment [3].

The main job of the lungs is to breathe in oxygen and exhale carbon dioxide when carrying out vital biological processes. Tissue and cell proliferation in the lungs goes unchecked and lead to lung cancer. These masses can spread and harm nearby tissues if they are allowed to grow out of control in their surroundings [4] Lung cancer is caused by unchecked cell growth, which results in the development of lung nodules [5]. Based on the properties of the cells, lung cancer can be divided into two main groups: small and non-small cell.[6]

Computed tomography (CT)scans,positron emission tomography (PET), magnetic resonance imaging (MRI),Chest radiographies (CXRs) and cytology sputum are among the diagnostic methods used to treat lung cancer. These techniques also have some drawbacks. For example, CT, Septum, and CXR are radiation-prone, and MRI and PET are less effective at detecting and staging lung cancer [7].The wavelet is used to examine the cancer cells and fuse the final image. Additionally, prediction techniques are used to determine whether a person's habits can influence their risk of developing cancer [8].The delicate character of pulmonary tissue can also make an accurate early diagnosis challenging, making biopsies and X-ray-based imaging difficult. If blood oxygen levels are low during the diagnosis, oxygen therapy is also recommended [9]. A bronchoscopy and lung biopsy are also painful, invasive procedures that should not be performed carelessly, even though they can accurately identify tumour cells.[10] Lung cancer disease is difficult to diagnose from CT scans. These days, Low-Dose Helical Computed Tomography (LDCT) is used as a modality for lung cancer screening [11]. The ability to classify lung cancer in its initialphases and differentiate it from tuberculosis makes image processing techniques extremely valuable in the fight against lung cancer. If the detected tumour growth turns out to be malignant, it can be easily removed, increasing the likelihood that a patient will survive [12].

The accurate fuzzy inference system (FIS) can be used to practically identify cancer by removing symptoms that are not relevant and addressing the primary symptoms from a temporal perspective. Because FIS has the highest accuracy and precision, it is widely used in a variety of systems and devices, both medical and non-medical [13]. A fuzzy rule-based expert system consists of a membership function and a set of fuzzy rules, in which subject matter experts can offer helpful guidance on acquiring new knowledge. Thus far, numerous sciences have witnessed an increasing research focus on the fuzzy inference system [14]. This information can be used to detect and diagnose lung cancer by incorporating it into a fuzzy expert system. The aim of this work is to develop an expert system for lung cancer diagnosis based on fuzzy rules [15].

The major contribution of this work are as follows:

- A novel contribution to the field of feature ranking is the introduction of a Modified Fuzzy AHP that includes sigmoid membership functions tailored for each feature.
- A novel and distinctive method is presented by the hybrid ChimpGaz optimization algorithm, which combines the optimizations of Gazelle and Chimp. This algorithm optimizes parameter

configurations and improves ROI division precision by fine-tuning the Mask R-CNN for ROI identification.

- The distinct feature of the proposed detection model, "FuzSquResMobileNet," is its combination of a complex ensemble of pre-trained deep learning models with fuzzy logic-based preliminary detection.

The structure of this study is as follows: Section 2 represents a review of the relevant literature. Section 3 delves into the proposed method, and Section 4 discusses the attained outcomes. Lastly, Section 5 concludes the paper.

2. Literature Survey:

"Some of the recent study related to lung cancer detection were reviewed in this section"

Khalil, *et al*., (2020) [16] have created a novel fuzzy soft expert system to forecast the occurrence of lung cancer. There were four primary steps involved in the forecast process with this fuzzy soft expert system: (1) Real-valued inputs were transformed into fuzzy numbers. (2) Fuzzy soft sets were created from the fuzzy numbers in the data. (3) The normal parameter reduction method was used to reduce the resulting fuzzy soft set family into a new fuzzy soft set family. The suggested algorithm was applied in order to acquire the resultant data. 45 patients, 15 females and 30 males who were receiving treatment in the respiratory department of Nanjing Chest Hospital in China participated in an experiment. All of the patients were cigarette smokers.

Palani, and Venkatalakshmi, (2019) [17] have suggested an approach for Internet of Things (IoT)-based modelling of prediction that can be used to predict the occurrence of lung cancer disease: fuzzy cluster-based enhancement and classification. through continuous surveillance and enhance healthcare by delivering medication instructions. For efficient image segmentation, they used the fuzzy clustering technique, that uses transition region extraction as its foundation. Fuzzy C-Means Clustering was also used to classify transitional region features from lung cancer image characteristics. The Otsu thresholding technique was utilized to extract the transition region from images of lung cancer. Additionally, the segmentation performance was improved by using the morphological thinning operation and the right edge image.

Hatuwal, and Thapa, (2020) [18] have presented lung cancer recognizing using histopathological images. For diagnosis, doctors used histopathological pictures of tissue biopsies from possibly infected lung regions. CNN were used to quickly and more accurately identify and classify different types of lung cancer, which is important for choosing the best course of treatment and increasing patient survival. An image was classified into three categories using a CNN: benign, adenocarcinoma, and squamous cell carcinoma.

Mishra., *et al*., (2021) [19] have offered as a way to combine computational intelligence with the Internet of Health Things (IoHT) to detect lung cancer.The random forest algorithm is used to classify and distinguish lung cancer patients from healthy individuals after the heuristic Greedy Best First Search (GBFS) algorithm has selected the most pertinent attributes from the lung cancer data. A sustainable prototype approach to the treatment of lung cancer was created by utilizing the most recent technological advancements in the form of computational intelligence and the Internet of Things. This

study develops an IoHT-based lung cancer detection model that is both automated and computationally intelligent.

Jalaldeen, *et al*., (2021) [20] have developed a technique for segmenting images using Gaussian mixture models and the Mean-Shift Clustering Algorithm. A mode-seeking algorithm was implemented using mean shift, a non-parametric feature-space analysis technique to find the maxima of a density function. Using the new advanced CT scan, the suspicious region of the lung tumor was reduced by applying the multi-level classifier segmentation technique that was proposed. In addition, a novel fuzzy-based multi-level classifier was presented that uses extracted textural features to classify CT scan snapshots.

Prasad, J., *et al*., (2022) [21] have suggested a segmentation strategy for lung cancer. After the input CT image underwent pre-processing to remove noise, texture features were obtainedfrom the processed image. The crow search optimization algorithm was used to select features in the following phase. Later, the distinction between abnormal and normal lung images was made using an artificial neural network. Ultimately, abnormal images were segmented separately using the fuzzy K-means algorithm. An SVM classifier was employed in the second phase to lower the number of false positives.

Tiwari, *et al*., (2021) [22] have presented a successful Target-based Weighted Elman DL Neural Network (TWEDLNN) and Mask Unit (MU) based 3FCM algorithm-based Deep Learning (DL) method for the detection of lung cancer. The study suggested included the following: contrast enhancement (CE) using Modified Clip limit-based (MC-CLAHE), feature extraction (FE), feature classification using TWEDLNN, lung image segmentation using Geometric mean-based Otsu Thresholding (GOT), and MU based FCM algorithm for LN (lung nodule) detection. For the implementation, CT scans from the LIDC-IDRI database were used.

Lakshmanaprabu, *et al*., (2019) [23] have presented a novel automated diagnosis classification technique for lung CT (Computerized Tomography) images. The Linear Discriminant Analysis (LDA) and Optimal Deep Neural Network (ODNN) were used to analyse CT scans of lung images. To classify lung nodules as benign or malignant, deep features were obtainedfrom CT images and their LDA was employed to minimize dimensionality. The Modified Gravitational Search Algorithm (MGSA) was utilized to optimize the ODNN on CT images in order to categorize lung cancer.

Hussain, *et al*., (2019) [24] havesuggested a system that was created by combining deep learning with fuzzy K-means clustering.Multiscale fuzzy entropy (MFE),Multiscale permutation entropy (MPE),proposed multiscale sample entropy (MSE) with a mean and KD-tree algorithmic approach,refined composite MFE (RCMFE) with mean, standard deviations and variance are among the approaches used to segment tumours from CT lung images that combine deep learning and FKM approach.

Masood, *et al*., (2020) [25] have offered a refined multidimensional autonomous decision support system for lung nodule identification and categorization that is based on the Region-based Fully Convolutional Network (mRFCN). The mRFCN was used in conjunction with the innovative multi-Layer fusion Region Proposal Network (mLRPN) with position-sensitive score maps (PSSM) under investigation as an image classifier backbone for feature extraction.The architecture was modified to incorporate a deconvolutional layer in order to use the recommended mLRPN for automatically

choosing potential ROI. In order to utilize the three-dimensional data from CT scans, a median intensity projection was utilized.

2.1. Problem statement

In the field of lung cancer diagnosis and detection, the literature provides a thorough examination of the many approaches and strategies used. All of these studies have as their common issue the urgent need for reliable and effective lung cancer detection techniques. Because lung cancer has a high death rate and is a major global health concern, it is imperative that new diagnostic techniques be developed. The studies cover a spectrum of approaches, ranging from fuzzy soft expert systems for prediction to deep learning-based methodologies, and integration of computational intelligence with the IoT.The difficulties of accurately classifying various forms of lung cancer, the decrease of false positives in detection systems, and the intricacies of image segmentation in CT scans are among the challenges addressed. To improve overall lung cancer detection accuracy, novel approaches like fuzzy clustering, CNN, and hybrid optimization algorithms are included in the suggested solutions. The use of innovative technologies like IoT and computational intelligence, along with the combination of fuzzy logic and deep learning, demonstrate the diverse approaches taken to address the difficulties presented by a lung cancer diagnosis. The combined goal of these research projects is to help with early identification, accurate categorization, and eventually better results for lung cancer patients.

3. Proposed Methodology

The research proposes a methodology for lung cancer detection that is seamlessly integrated and begins with sophisticated methods for pre-processing to enhance quality of the images. Effective pre-processing is achieved by combining Gaussian filters with a modified Contrast Limited Adaptive Histogram Equalization (CLAHE) technique. Then, an optimized Mask R-CNN algorithm recognizes the Region of Interest (ROI), and a hybrid optimization algorithm that combines Chimp and Gazelle optimizations fine-tunes the hyper-parameters. For precise ROI segmentation, this guarantees ideal parameter settings. A wide range of features are covered by feature extraction, including texture features (Local Directional Patterns, or LDP, and Gabor Local Binary Patterns, or GLBP), color features (histograms), geometric features (centroid, Euler number, and convexity), and shape features (area, perimeter, and circularity). A Modified Fuzzy Analytic Hierarchy Process (AHP) with sigmoid membership functions customized for each feature is then used to rank the extracted features. To improve discriminatory power, a hybrid optimization algorithm that combines Chimp and Gazelle optimizations refines the membership functions. The final detection model, called "FuzSquResMobileNet," combines a group of pre-trained deep learning models (SqueezeNet, ResNet101, and MobileNetv2) with fuzzy logic-based preliminary detection to ensure a comprehensive approach to feature extraction for increased detection accuracy. The overall flow of the proposed lung cancer detection framework is illustrated in the figure 1.

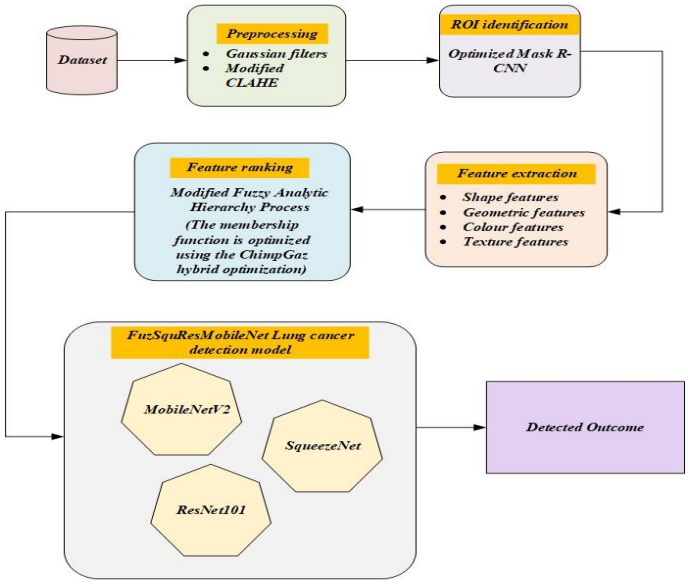

Figure 1: The proposed lung cancer overall detection framework

3.1. Pre-processing

Effective pre-processing methods are designed to enhance an image's quality and usefulness so that it can be used more effectively for tasks like feature extraction, object recognition, and segmentation. CLAHE and Gaussian filters are two pre-processing methods that are frequently used. The Gaussian Distribution Function is used by Gaussian filters, which are an effective tool for noise reduction. They smooth or blur an image by applying a weighted average technique. This effectively eliminates high-frequency noise components. The over-amplification problems with conventional Adaptive Histogram Equalization (AHE) are addressed by the CLAHE algorithm. The histograms are clipped in accordance with a defined clip limit to avoid over-amplification. A more balanced depiction of pixel intensities is ensured by redistributing clipped pixels as part of the process.

(i) Gaussian Filter

The noise of an image can be eliminated by applying a Gaussian filter. Each member of the linear filter has a weighting value. The high frequency component of the image is eliminated by this low pass filter. The image is blurred or smoothed by this filter using the Gaussian Distribution Function. The Gaussian filter's standard deviation indicates how much smoothing is applied. Weighted average is used in its operation, whereby the central pixel of the image is assigned greater weight than its surrounding pixels. A two-dimensional array at $[x, y]$ is used to represent the Gaussian filter. The Gaussian filter is represented in the equation (1).

$$G(x, y) = \frac{1}{2\pi\sigma^2} e^{-\frac{x^2+y^2}{2\sigma^2}} \quad (1)$$

Where σ indicates a standard deviation or sigma, and $G(x, y)$ indicates an element of the Gauss matrix at position $[x, y]$. The Gauss matrix's size, denoted by the values x, y provides the points x to $+x$ and its middle points at $y = 0$ and $x = 0$.

(ii) Modified CLAHE

A type of algorithm known as Adaptive Histogram Equalization, or AHE, is CLAHE. By utilizing the parameters for the clip limit and number of tiles, CLAHE addresses the over amplification issue with the traditional AHE.CLAHE divides the image into local tiles for MxN. The histogram is calculated for every tile separately. The average number of pixels in each region must first be determined using in order to calculate the histogram.

$$N_A = \frac{N_X \times N_Y}{N_G} \quad (2)$$

The number of pixels in the X dimension is N_X, the number of pixels in the Y dimension is N_Y, and the number of gray levels is N_G. The average number of pixels is N_A. After that, we can clip the histogram by defining the clip limit as in Eq. (2).

$$N_{CL} = f(I) \times N_A \times N_{NCL} \quad (3)$$

The clip limit (N_{CL}) and the normalized clip limit (N_{NCL}) between 0 and 1 are defined in Eq. (3). $f(I)$ function uses the local image characteristics to capture the variability in the clip limit. Pixel values, gradients, and any other pertinent image features may be taken into account by this function.The choice of this function depends on the specific characteristics you want to emphasize in determining the clip limit. The function can raise the clip limit for areas of the image that have sharper transitions or higher contrast. On the other hand, areas with softer transitions or less contrast might have a lower clip limit.With this modification, the CLAHE algorithm can now adapt better to various image structures and perform contrast enhancement more sensitively to the unique properties of the local regions within the image. Next, using Eq. (4), the clip limit is applied for each tile's height of the histogram.

$$H_i = \begin{cases} N_{CL} & if\ N_i \geq N_{CL} \\ N_i & else \end{cases} i = 1,2,\ldots.,l-1 \quad (4)$$

L is the number of gray levels, H_i is the height of the ith tile's histogram, and N_i is the ith tile's histogram. Equation (5) can be used to calculate the total number of clipped pixels.

$$N_C = (N_X \times N_Y) - \sum_{i=0}^{L-1} H_i \quad (5)$$

Where number of clipped pixels is N_C. The clipped pixels must also be redistributed after N_C has been calculated. There are two possible distributions for the pixels: uniform and non-uniform. Eq. (6) is used to determine the number of pixels that need to be redistributed.

$$N_R = {}^{N_C}/_{L} \quad (6)$$

The number of pixels to be redistributed is denoted by N_R. After that, Eq. (7) is used to normalize the clipped histogram.

$$H_i = \begin{cases} N_{CL} & if\ N_i + N_R \geq N_{CL} \\ N_i + N_R & else \end{cases} i = 1,2,\ldots.,l-1 \quad (7)$$

Equations (4) and (5) are used to calculate the number of undistributed pixels. Eq. (6) is repeated until all of the pixels have been redistributed. Finally, Eq. (8) can be used to express the contextual region's cumulative histogram.

$$C_i = \frac{1}{(N_X \times N_Y)} \sum_{j=0}^{i} H_j \quad (8)$$

The contextual region's histogram is matched with uniform, Rayleigh, or exponential probability distributions once all computations have been finished, giving it a preset brightness and visual quality. Assume that we have a pixel $P(x, y)$ with a value of s and that its four centre points R_1, R_2, R_3, and R_4 belong to the neighbouring tiles. These four contextual regions are combined to create a weighted sum.

3.2. ROI identification

ROI must be identified and precisely defined as a necessary first step. This work introduces an advanced approach to ROI identification, employing an optimized Mask R-CNN (Region-based Convolutional Neural Network) algorithm. Mask R-CNN is an effective tool that combines object detection and instance segmentation in a smooth way, making it possible to locate and define the boundaries of multiple objects within an image. This work further refines the hyper-parameters of the algorithm by integrating a hybrid optimization algorithm, thereby improving ROI segmentation accuracy. Chimp and Gazelle optimization methods are uniquely combined in the hybrid optimization algorithm.

(i) Mask R-CNN

Mask R-CNN is a prominent methodology for segmentation, capable of not only delineating a bounding box around a targeted object, but also discerning and categorizing whether the pixels contained therein pertain to the object or not. This ability facilitates object identification, boundary outlining, and key point detection. Mask R-CNN builds upon Faster R-CNN and increases its application in image segmentation. Region proposal networks (RPNs) are used by Faster R-CNN and Mask RCNN for feature extraction, data classification, and bounding box tightening. Faster R-CNN employs ROIPool as a feature extraction technique for quantifying each ROI region and using maximum pooling to address the issue of the sizes of ROI features at various scales. However, the method results in the loss of spatial information, misplacing the ROI and extraction properties of the original image. Mask R-CNN uses ROI alignment (ROIAlign) in place of Faster R-CNN's ROI pooling to address this issue, and then uses the mask branch to sequentially mark the ROI alignment result for the object region. After the network design was finished, a radiologist-drawn tumor contour was used as ground truth to train the Mask R-CNN on the images, the accompanying biopsy data, and the tumour contours. The data from the training set was employedto build a model, which was then evaluated against the validation set to make sure it was accurate and stable. The training method randomly divided the cases into a training and a validation set. The RPN training loss and the multibranch prediction network training loss make up the majority of the Mask R-CNN's training loss in terms of the loss function. The following equation (9) is the training total loss $L_f$calculation formula:

$$L_f = L_{RPN} + L_{Mul.Branch} \quad (9)$$

where L_{RPN} consists of the rectangular box regression loss (smooth L_1 loss) and the anchor classification loss (softmax loss). The LRPN is determined as per the equation (10):

$$L_{RPN} = \frac{1}{N_{cls1}} \sum_i L_{cls}(p_i, p_i^*) + \gamma_1 \frac{1}{N_{reg1}} \sum_i p_i^* L_{reg}(t_i, t_i^*) \quad (10)$$

where $L_{Mul.Branch}$ is the total of the three branch losses in the multitask prediction network (softmax loss, smoothing L1 loss, and mask loss):

$$L_{Mul.Branch} = L(p_i, p_i^*, t_i, t_i^*, s_i, s_i^*) \quad (11)$$

$$L_{RPN} = \frac{1}{N_{cls2}}\sum_i L_{cls}(p_i, p_i^*) + \gamma_2 \frac{1}{N_{reg2}}\sum_i p_i^* L_{reg}(t_i, t_i^*) + \lambda_2 \frac{1}{N_{mask}}\sum_i L_{mask}(s_i, s_i^*) \quad (12)$$

The constant N_* denotes the quantity of comparable anchor points or rectangular boxes in Equations (11) and (12). The balanced mask loss and rectangular box regression loss, respectively, are hyperparametersλ_* andγ_*.The following formulas (13) –(16) are used to derive the classification loss L_{cls}, regression loss L_{reg}, and mask loss L_{mask}:

$$L_{cls}(p_i, p_i^* p_i) = -log p_i^* p_i \quad (13)$$

$$L_{reg}(t_i, t_i^*) = smooth_{L_1}(t_i^* - t_i) \quad (14)$$

$$smooth_{L_1}(x) = \begin{cases} 0.5\, x^2 & if\ |x| < 1 \\ |x| - 0.5 & otherwise \end{cases} \quad (15)$$

$$L_{mask}(s_i, s_i^*) = -(s_i^* \log(s_i) + (1 - s_i^*)\log(1 - s_i)) \quad (16)$$

where p_i^* is the ground-truth label probability and p_i is the classification probability of anchor i. The variable represents the difference between the ground-truth label box and the predicted rectangle box using four parameter vectors: the height, and width vertical and horizontal coordinates of the points in the rectangle.Optimizing the values of γ_1, γ_2 and λ_2 hyperparameters will maximize performance by adjusting the ratios of the rectangular box regression loss, anchor classification loss, and mask loss, correspondingly.By adjusting these parameters with the help of the hybrid optimization algorithm, the Mask R-CNN model is customized to the unique properties of the data, improving the accuracy of ROI segmentation.

(ii) ChimpGaz optimization algorithm

The ChimpGaz optimization algorithm is a hybrid optimization technique that blends the distinctive features of the Chimp optimization algorithm, which draws inspiration from the collective intelligence and hunting behaviour of chimpanzees, with the search strategy of the Gazelle algorithm, which draws inspiration from the guided movement and foraging habits of gazelles.Gazelle optimization brings speed and efficiency to the fine-tuning process, while Chimp optimization adds flexibility and comprehensive exploration of the hyper-parameter space work together to find the ideal configuration of these hyper-parameters. The combination of these optimization methods improves Mask R-CNN's overall performance by allowing the algorithm to better adapt to the complexity of various datasets and successfully identify and distinguish ROIs in a variety of images.

(a) Chimp Intelligence Imitation Phase

The sexual motivation and individual intelligence of chimpanzees in their collective hunts are the inspiration for a new algorithm that draws inspiration from nature. This algorithm is known as the Chimp optimisation algorithm (ChoA) method. Comparable social predators cannot compare to it. To simulate several types of intelligence, including barrier, attacker, driver and chaseramong others, this

methodology comprises four distinct phases. The following mathematical equations (Eqs. ((17)-(18)) illustrate the driving and chasing of the target or prey:

$$D = \left|c.y_{prey}(k) - \ m.y_{chimp}(k)\right| \quad (17)$$

$$y_{chimp}(k+1) = \ y_{prey}(k) - \ a.d * \mu * \overrightarrow{R_l} \quad (18)$$

where c, m, and a are the coefficient vectors. Eqs (19-21) calculate the coefficients $c, m,$ and a.

$$a = 2.h.r_1 - h \quad (19)$$

$$c = 2.r_2 \quad (20)$$

$$m = \ chaotic_{value} \quad (21)$$

where y_{chimp} is the current chimp position vector and y_{prey} is the prey position vector; As the number of iterations increases, the convergence factor, h, declines nonlinearly from 2.5 to 0 (including the exploration and exploitation phases). The distance between the chimp and the prey is indicated by the random vector a, whose value is a random number between $[-2\ h, 2\ h]$. The distance between the chimp and the prey is denoted by d, while the number of iterations is represented by k. Random vectors between [0,1] are represented by r_1 and r_2.c is a random vector in the range of $[0, 2]$ that controls the chimp's driving and chasing of the prey; when $|a| < 1$, the chimp's position tends to approach that of the prey y_{prey}; When $|a| > 1$, the chimp is compelled to move away from the prey's location and conduct a broader search for the prey. The chimp position is affected by the prey position less when c is less than 1, and more otherwise.The effect of individual motivation on the chimp's location during the hunting process is represented by the chaotic vector m, which is computed from different chaotic mappings. The inclusion of the parameter 'μ' inspired from the gazelle signifies abrupt directional changes in the chimp's movement during each iteration. This alternating direction movement, which is seen in odd and even iterations, is similar to Lévy flight behaviour, which helps the chimp locate the prey quickly and exploratorily. The chimp's movement is further given stochasticity by the vector $\overrightarrow{R_l}$ derived from Levy distributions from the gazelle behaviour, which broadens its search strategy.

(b) Chimpanzee Predatory Behaviour (Exploitation Phase)

In this step, the chimpanzees' behaviour has been mathematically implemented. Since they are more knowledgeable about the target's location, it is assumed that the barrier, attacker, chaser and driver can provide the first response in this case. The remaining chimpanzees are made to update their own positions in accordance with the best chimpanzee locations in the following iteration when four additional optima solutions have been acquired and are kept. These mathematical equations serve as examples of this procedure. (22) – (25):

$$d_{attacker} = \ |c_1 y_{attacker} - \ m_1 z| \quad (22)$$

$$d_{barier} = \ |c_2 y_{barrier} - \ m_2 z| \quad (23)$$

$$d_{chaser} = \ |c_3 y_{chaser} - \ m_3 z| \quad (24)$$

$$d_{driver} = \ |c_4 y_{driver} - \ m_4 z| \quad (25)$$

If the random vectors fall within the range of [1, 1], then the chimpanzee's future position can be at any location between the present location and the location of the target or prey.

$$z_1 = y_{attacker} - y_1.d_{attacker} \quad (26)$$

$$z_2 = y_{barier} - y_2.d_{barier} \quad (27)$$

$$z_3 = y_{chaser} - y_3.d_{chaser} \quad (28)$$

$$z_4 = y_{driver} - y_4.d_{driver} \quad (29)$$

(c) Gazelle-Inspired Search Strategy

The Brownian motion, which is typified by uniform and controlled steps, is effectively used during this phase to cover neighbouring regions of the domain. The following mathematical Eq. (30) updates the chimpanzees' location during the search procedure using the overall equations:

$$z_{n+1} = \frac{z_1 + z_2 + z_3 + z_4}{4} * S.R * R_b \quad (30)$$

where S is the somersault factor, which is used to determine the somersault range, which is $S = 2$. Constant random integers [0, 1] make up the vector R_b, and R is a vector of various random numbers that exhibit the Brownian motion inspired from the gazelle optimization.

(d) Fibonacci Search Method (FSM) Integration

The Fibonacci search method is the one that, after a finite number of tests are run, produces the smallest uncertainty interval in which the best solution is found.The Fibonacci numbers (Fib) sequence, as displayed by Equation (10), serves as the foundation for the Fibonacci search.

$$F_0 = 1 = F_1, F_k = F_{k-1} + F_{k-1} + F_{k-2}, k = 2,3,4 \ldots., n$$

The FSM is an approach to solving non-linear optimization problems that is also known as the interval reduction method or elimination technique. To find the extreme value of functions, the FSM uses Fibonacci numbers to shift and narrow the search range.This technique enhances the updated equation of gazelle inspired search by employing the Fibonacci search method (FSM), which is cantered on updating the best solution currently found during the iterative process. The FSM guarantees that the solutions are not confined to local optima and encourages a high degree of diversification.

$$y_{chimp}(k+1) = z_{n+1} + \left(\frac{F_{k-2}}{F_k}\right)(b_i - a_i) \quad (31)$$

Fibonacci sequence-based FSM is integrated to enhance search process, update solutions, and guarantee that the algorithm explores a wide range of solutions instead of being limited to local optima.In order to accomplish effective optimization in difficult problem spaces, this algorithm appears to be designed to strike a balance between exploration and exploitation by leveraging various mechanisms that are inspired by nature.

(e) Dynamic Chaotic Movement

In order to simulate this simultaneous behaviour, the assumption is made that there is a 50% chance that the chimp's position will be updated during optimization via the chaotic model or the

regular updating mechanism. Ultimately, the location of the chimpanzees within the search domain has been updated using the subsequent mathematical equation (32):

$$y_{chimp}(k+1) = \begin{cases} y_{prey}(k) - z.d & if\ \phi < 0.5 \\ chaotic\ value & if\ \phi > 0.5 \end{cases} \quad (32)$$

Where $\phi$is a random number between [0,1]. When determining whether to move closer to the prey or rely on chaotic values to guide its movement, the final location update takes into account a random numberϕ. The last stage of this chaotic behavior aids chimps in overcoming the two issues of being trapped in local optima and having a slow rate of convergence when solving high-dimensional problems. The ChimpGaz optimization algorithm is essential for optimizing the Mask R-CNN algorithm because of its capacity to adjust to a variety of datasets, thoroughly explore hyper-parameter spaces, and converge quickly. This improvement ultimately leads to enhanced accuracy in ROI segmentation which subsequently raises the overall efficacy of lung cancer detection frameworks. Figure 2 shows the pre-processed and ROI identification of sample images.

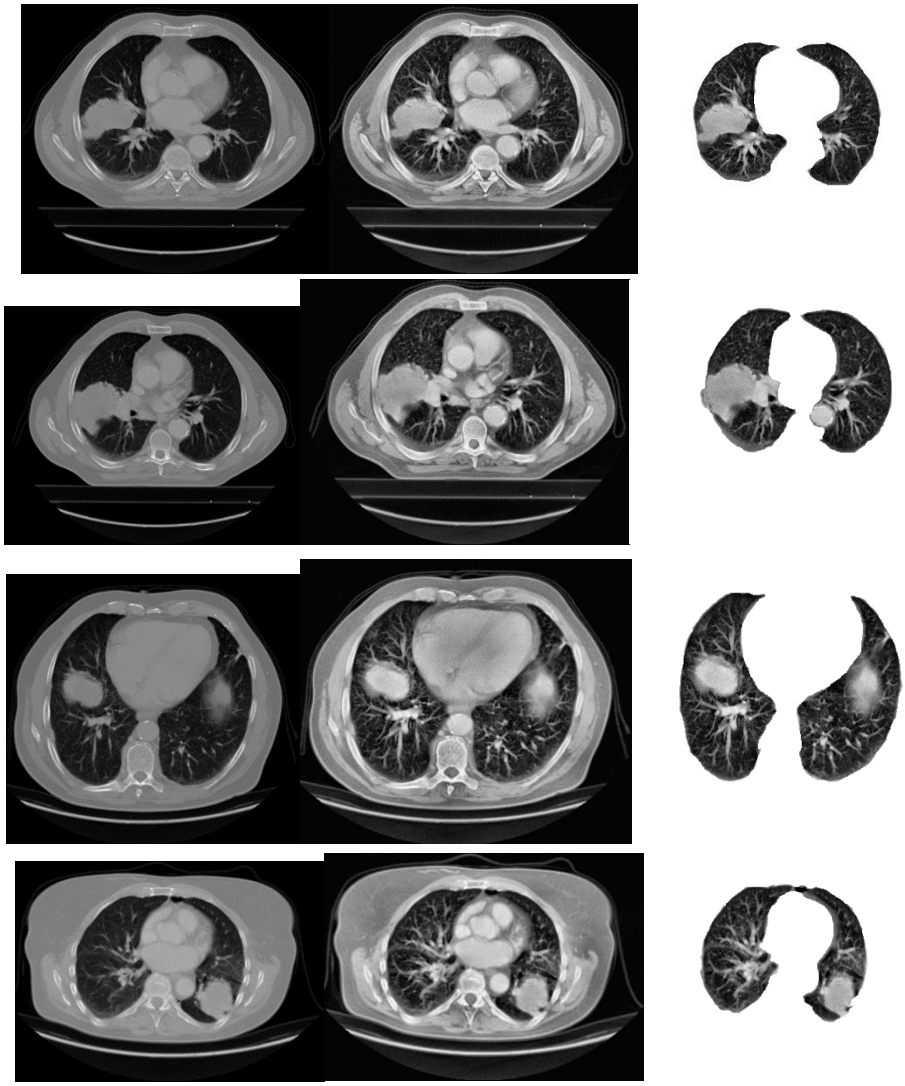

Input images **Pre-processed images** **ROI identified images**

Figure 2: Sample images of pre-processed and ROI identified images

3.3. Feature extraction

Feature extraction, which involves extracting crucial data from medical images to enable precise analysis, is a crucial stage in the recognitionof lung cancer. A wide range of descriptors are used in this work, including shape features (circumference, area, and perimeter), geometric features (centroid, Euler number, and convexity), color features (histograms), and texture features (Local Directional Patterns, or LDP, and Gabor Local Binary Patterns, or GLBP). Each of these methods is essential for obtaining pertinent data that is useful for identifying minute details indicative of lung cancer.

3.3.1. Shape features

The analysis and characterisation of regions inside images depend heavily on the computation of shape and geometric properties, such as area, perimeter, and eccentricity. These properties offer useful details about the size, shape, and contour of objects, which can be used in a variety of applications.

(i) Area

The actual number of pixels in the image region can be used to calculate the area. Every pixel has a unique weight. This value deviates from the binary image area.

$$Area = \pi * radius^2 \quad (33)$$

(ii) Perimeter

The number of pixels along the image's edge or margin can be used to calculate the perimeter.

(iii) Circularity

The roundness or circularity (area-to-perimeter ratio), which removes local irregularities, can be found by dividing an object's area by the area of a circle with the same convex perimeter.

$$Circularity = \frac{4\pi.area}{(perimeter)^2} \quad (34)$$

3.3.2. Geometric features

The centroid denotes the centre of mass, the Euler number describes topological characteristics, and convexity measures the degree of concavity in a region. These geometric features add to a more comprehensive understanding of the spatial relationships between various tissue components.

(i) Convexity:

The convex object has a convexity value of 1. Any convex curve with a value of less than one with respect to the object is regarded as having an irregular boundary. The following equation gives the convexity formula.

$$Convexity = \frac{Convexity\ perimeter}{Perimeter} \quad (35)$$

(ii) Euler number

The Euler number describes the relationship between the number of holes on a shape and the number of contiguous parts. Let S represent the number of adjacent parts and N represent the number of holes on a shape. The Euler number is thus:

$$Eul = S - N \quad (36)$$

(iii) Convexity

Convexity quantifies how "rounded" or "convex" a shape is. The smallest convex shape enclosing an object is its convex hull. The area of the convex hull divided by the area of the object is known as the convexity. The convexity of an object that is perfectly convex is 1.

3.3.3. Colour features

Analysing pixel intensities and the position within medical image datasets is necessary for color features. A quantitative depiction of pixel intensities across various color channels is offered by histograms. This method is essential for identifying color changes in tissue, which may be a sign of abnormalities.

3.3.4. Texture features

Texture features highlight the smaller details in the images, bringing to light patterns that the naked eye might miss. Techniques that are excellent at identifying minute differences in texture are Local Directional Patterns (LDP) and Gabor Local Binary Patterns (GLBP). Local texture patterns are characterized by LDP using directional information, whereas GLBP combines binary pattern encoding and Gabor filtering.

(i) Local Directional Pattern

The Local Directional Pattern (LDP) technique fared better than the LBP technique. Compared to LBP, LDP is more resilient to noise and non-monotonic variations in illumination because it relies on edge responses, which are more stable than intensity values. The LDP determines the pixel's eight-directional edge responses in each direction. A high edge response value in either direction would suggest the existence of an edge. Therefore, the most prominent directions are encoded using the top-k directional bit responses.The top-directional bits are assigned a value of "1," while the remaining bits are allocated a value of "0."For each pixel, the LDP code is as follows:

$$LDP_k = \sum_{i=0}^{7} b_i(m_i - m_k) * 2^i, b_i(x) \quad (37)$$

Where m_k represents the directional response that is k-th most significant.

(ii) GLBP

The Local Binary Pattern (LBP) descriptor, a grayscale invariant measure based on an overall description of the texture in a local neighborhood, is a quick and easy way to represent texture characteristics.The process involves establishing two parameters: R and P. R stands for the radius (distance) measured from the source pixel, and P is the number of neighbors used to compute LBP.

$$LBP_{P,R}(x_C, y_C) = \sum_{P=0}^{P-1} s(g_p - g_c)2^P \quad (38)$$

Where x_C and y_C represent the location of the interest pixel in the image. The central pixel value is indicated by g_p.g_c denotes the value of the central pixel's circular neighbors, and 2^P denotes the weight given to each operation between the neighbor and the central pixel. Finally, values of 1 and 0 are assigned to $s(g_p - g_c)$.

The gabor filter uses particular trignometric operations to extract data at various orientations in order to gather texture information from an image.In terms of trignometric functions of θ, A pair of tuples of data indicating x and y is the definition of the gabor G, which stand for the axis that the texture data is oriented along.The gabor filter has a filter coefficient that filters an image's spatial coordinates at various angles between 0 and 2π.

$$g(x, y, \theta, \xi) = I(x, y)W(x, y) + \theta + \xi \quad (39)$$

where an object's edges and boundaries in an image are described by a scalar variable, θ. An image with spatial coordinates is denoted by $I(x, y)$, and the filter coefficients $W(x, y)$ are employed to filter the intensities at each pixel in relation to the weights allocated to it.The parameters θ and ξ are used to extract fine-grained, detailed information from images at various angles of edges and boundaries oriented within images, respectively. ξ is used to acquire textured data with greater detail. As shown in equation 40, the parameter θ is expressedin terms of the trigonometric functions $sine\ \theta$ and $cos\ \theta$.

$$angle(\theta) = xcos\ \theta + ysine\ \theta \quad (40)$$

$$\xi = \prod(w(x, y), radius(1) + w(x, y), radius(2)) \quad (41)$$

$$f_{i,j} = \sum_{P=0}^{P-1} s(g_p - g_c)2^P + I(x, y)W(x, y) + \theta + \xi \quad (42)$$

Equation (2) carries out the task of determining the alignment of pointsand lineson an image's boundaries and edges, while Equation (3) uses a Gabor filter to extract additional information from an LBP at various radii.Since identifying lung cancer requires extracting a more thorough description of an image, the result of LBP is cascaded with Gabor filter G to provide more texture-specific information about an image. Cascading the LBP texture information acquired in the form of bins with a Gabor filter allows additional information about an image to be extracted. These texture characteristics have the advantage of highlighting small characteristics, like slight alterations in tissue texture or microstructural patterns, that are essential for identifying early indicators of lung cancer.

The combined use of shape, geometric, colour, and texture features ensures a holistic approach to feature extraction, capturing a diverse range of information from lung images. In order to extract multifaceted information from medical images, these techniques have been integrated.

3.4. Feature Ranking

Feature ranking, which aims to identify the most relevant features that significantly contribute to the accurate classification of medical images, is an important step in the lung cancer detection process. A sophisticated method is used in this work, which uses a Modified Fuzzy Analytic Hierarchy Process (AHP) to rank features. This approach uses sigmoid membership functions that are customized for every feature. To improve the discriminatory power, these membership functions are refined using a ChimpGaz hybrid optimization algorithm.

3.4.1. Modified Fuzzy Analytic Hierarchy Process

The Modified Fuzzy Analytic Hierarchy Process (Fuzzy AHP) combines fuzzy logic with the traditional Analytic Hierarchy Process to address vaguenessanduncertainties in decision-making. It presents the idea of representing and processing imprecise data using fuzzy sets and Pentagonal fuzzy numbers.

(i) Fuzzy set

The values of a fuzzy set $\tilde{A}_F$in the interval [0, 1] come from its domain or universe of discourse $\tilde{X}$, and it is defined by,

$$\tilde{A}_F = (x, \mu(x), x \in \tilde{X} \quad (43)$$

$$\mu(x) = \frac{1}{1+e^{-a(x-c)}} \quad (44)$$

Where $\mu(x)$ is the sigmoidal membership function.For every feature, sigmoid membership functions are used to capture the gradual change in importance levels. The S-shaped curve that typifies sigmoid functions enables a continuous and smooth depiction of the membership values. Each feature has its own set of functions that are specifically designed to highlight its distinct role in the task of detecting lung cancer.

(ii) Fuzzy number

A pentagonal fuzzy number (PFN) is $A = (z_1, z_2, z_3, z_4, z_5)$, where z_3 is the middle point and (z_1, z_2) and (z_4, z_5) are the points on the left and right sides of z_3, respectively. The membership grade of point z_3 is 1, and the grades of points z_2, z_4, and w_1, w_2 are the corresponding values. Each PFN has two weights, w_1, w_2, assigned to it. To prevent confusion, w_1 and w_2 are represented as the weights of the PFN A using the notationw_{iA} for $i = 1,2$.

The three operations that can be carried out on pentagon fuzzy numbers are as follows: assuming that the two pentagon fuzzy numbers are $\tilde{Y}_P = y_1, y_2, y_3, y_4, y_5$and $\tilde{Z}_P = z_1, z_2, z_3, z_4, z_5$.

Addition: $\tilde{Z}_P \oplus \tilde{Y}_P = (z_1 + y_1, z_2 + y_2, z_3 + y_3, z_4 + y_4, z_5 + y_5)$ (45)

Subtraction: $\tilde{Z}_P(-)\tilde{Y}_P = (z_1 - y_1, z_2 - y_2, z_3 - y_3, z_4 - y_4, z_5 - y_5)$ (46)

Multiplication: $\tilde{Z}_P * \tilde{Y}_P = (z_1 * y_1, z_2 * y_2, z_3 * y_3, z_4 * y_4, z_5 * y_5)$ (47)

Division: $\tilde{Z}_P \Big/ \tilde{Y}_P = (z_1/y_1, z_2/y_2, z_3/y_3, z_4/y_4, z_5/y_5)$ (48)

The PFN-AHP integrates fuzzy logic with the conventional AHP, as the latter does not account for uncertainty in individual reasoning. Linguistic variables are incorporated into fuzzy logic. Linguistic variables are those whose values are words as opposed to numbers.The suggested AHP in this instance makes use of PFN logic, which provides understanding of truth, unpredictability, and falsity of any linguistic variable. Therefore, refining the fuzzy logic approaches improves the convergence of AHP. The linguistic variables expressed in PFN-AHP have been used to obtain pairwise comparisons for criteria. The elements of a pairwise comparison matrix show the pairwise comparisons of various features. Assume a matrix C is created, and that the comparison value between features i and j is represented by the C_{ij}. That means that for a matrix of pairwise comparisons with pentagonal fuzzy numbers is given as

$$C = \begin{pmatrix} \mu_{11}(C_{11}) & \mu_{12}(C_{12}) & \dots & \mu_{1n}(C_{1n}) \\ \mu_{21}(C_{21}) & \mu_{22}(C_{22}) & \dots & \mu_{2n}(C_{2n}) \\ \vdots & \vdots & \ddots & \vdots \\ \mu_{n1}(C_{n1}) & \mu_{n2}(C_{n2}) & \dots & \mu_{nn}(C_{nn}) \end{pmatrix} \quad (49)$$

$$c_{ij} = (l_{ij}, m_{ij}, n_{ij}, s_{ij}, t_{ij}) \quad (50)$$

In this case, the crisp value for the comparison between features i and j is represented by a C_{ij} and the fuzzy number is represented by $\mu_{ij}(C_{ij})$ using the sigmoid membership function. A more sophisticated representation of ambiguity and uncertainty in the decision-making process is possible with this modified version of the Fuzzy AHP technique.

(iii) Determine the matrix's largest eigenvalue

The following formula can be used to determine the matrix's largest eigenvalue:

$$X_w = \lambda_{max} w \quad (51)$$

where w is the matrix's principal eigenvector.

(iv) Consistency check

The consistency ratio (CR), which is defined as follows, can be used to assess the consistency of the comparison matrix.

$$CR = \frac{CI}{RI} \quad (52)$$

$$CI = \frac{\lambda_{max} - n}{n-1} \quad (53)$$

where RI is the random index and CI is the consistency index. Pair-wise comparisons should be revised if the matrix's consistency is deemed acceptable, which usually happens only if the coefficient of determination (CR) is less than 0.10.

(v) Fuzzy Geometric Mean

Each criterion's fuzzy geometric mean is calculated using the equation (54).

$$\tilde{r}_i = \left(\prod_{j=1}^{n} c_{ij}\right)^{1/n} i = 1,2, \dots \dots, n \quad (54)$$

where c_{ij} is the group of decision-makers' fuzzy comparison value with respect to the i th dimension over the j^{th} criterion, and $\tilde{r}_i$ is the fuzzy geometric mean.

(vi) Fuzzy Weight and Defuzzification

Equation (5) calculates each criterion's fuzzy weight.

$$\widetilde{w}_i = \tilde{r}_i \times (\tilde{r}_1 + \tilde{r}_2 + \cdots \dots + \tilde{r}_n)^{-1} \quad (55)$$

The fuzzy weight should be defuzzied using the average weight criterion M_i using the equation (56).

$$M_i = \frac{\widetilde{w}_1 + \widetilde{w}_2 + \cdots \dots + \widetilde{w}_n}{n} \quad (56)$$

(vii) Normalized Weight Criteria

The weight criteria that are normalized N_i is determined using equation (57).

$$N_i = \frac{M_i}{\sum_{i=1}^{n} M_i} \quad (57)$$

A comprehensive framework for making decisions in the face of uncertainty is offered by the Modified Fuzzy AHP. Fuzzy logic is smoothly incorporated with the conventional AHP, enabling a more complex depiction of ambiguity and uncertainty. Decision-making processes are made more accurate and reliable by incorporating fuzzy geometric means and weights, PFNs, and linguistic variables. The robustness of the approach is ensured by the consistency check and normalization steps, which give decision-makers a reliable tool for difficult decision scenarios. Precise feature ranking is essential for lung cancer detection in order to choose the most informative features that have a major influence on the algorithm's decision-making. The improved discriminatory power obtained via the utilization of Modified Fuzzy AHP, sigmoid membership functions, and the hybrid optimization algorithm contributes to the overall precision and dependability of lung cancer detection systems.

3.5. FuzSquResMobileNet Lung cancer detection model

The FuzSquResMobileNet model combines components from ResNet 101, SqueezeNet, and MobileNet V2 in a meticulously designed architecture that takes advantage of the advantages of several convolutional neural network (CNN) architectures. The goal of this ensemble-based method is to develop a reliable and effective lung cancer detection model. The input Layer, which takes in the images from the previous stage of feature ranking, is where the model starts. Subsequently, the architecture includes ResNet 101's CONV 1, the first convolutional layer. The foundation for basic feature extraction is this layer. Three convolutional blocks from ResNet 101 make up the next layer, CONV3X, and each has residual connections. This configuration makes it easier to optimize during the training process and allows for deeper feature extraction. The architecture incorporates the SqueezeNet FIRE Module to enable effective feature processing. This module expands features and creates richer representations by using 1x1 and 3x3 convolutions to compress input channels and expand features, respectively. The model then goes through further feature processing through CONV4X (ResNet 101) and the FIRE Module, followed by further enhancement with CONV 23X (ResNet 101) and the FIRE Module. ResNet 101 blocks and SqueezeNet's FIRE module work together to balance computational efficiency and feature extraction capabilities.Thearchitecture further refines features with CONV 3x (ResNet 101) and the FIRE Module in the final ResNet 101 blocks. For computational efficiency, a Depthwise Separable Convolution layer from MobileNet V2 is also introduced. By factorizing convolutions, this layer lowers the number of parameters and speeds up inference. Then, to downsample feature maps and lower dimensionality and computational costs in later layers, average pooling is used. The Fully Connected (FC) layer, the last layer in the architecture, combines the learned features to generate the output of the model. This output layer is probably a representation of class probabilities in the framework of lung cancer detection, enabling to classify lung cancer or other pertinent diagnostic results. The proposed FuzSquResMobileNet Lung cancer detection model is shown in the figure 3.

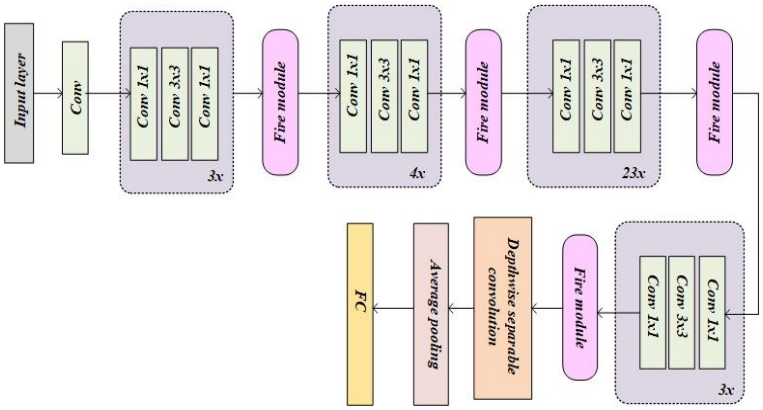

Figure 3: Proposed FuzSquResMobileNet Lung cancer detection model

A convolutional neural network with 101 deep layers is called ResNet-101 (Residual Network 101). A network's accuracy quickly degrades after it becomes saturated as its depth rises. Deeper networks exhibit the vanishing gradient, which is the source of accuracy degradation. ResNet fits a residual mapping to these layers instead of adding each stacked layer individually. It bypasses one or more layers by using a shortcut connection. The outputs of the stacked layers are multiplied by the outputs of the shortcut connections, and they carry out identity mapping. To reach the final destination, the value will be added to the input through residual mapping. Deeper ResNet networks use a bottleneck design. ResNet101 has 104 convolutional layers, which are made up of 33 blocks of layers. 29 of these squares are used directly in earlier blocks. A convolution layer, a max pooling layer with a stride of 2, 33 residual building blocks, and a pooling layer with a stride of 7 make up the residual model. For every residual function, a stack of three convolutional layers1x1, 3x3, and 1x1 layersis created. The 1x1 convolution layers are employed for minimizing and then recovering the dimensions. The 3x3 layer, on the other hand, has smaller input and output dimensions and acts as a bottleneck.ResNet modifies the input layer using batch normalisation to improve network performance.

The Squeeze Net network is made up of Fire modules, which are building pieces. There are two layers in every fire module: an expand layer and a squeeze layer. The expand layer combines 1x1 and 3x3 maps, and the squeeze layer is just a layer of 1x1 convolution maps. Squeeze layer feature map counts are set to be less than or equal to those of the expand layer feature maps, which results in a compression of the extracted feature maps and a decrease in the number of network weights. The microarchitecture of the Squeeze Net model is then constructed by stacking these Fire modules together. The number of Squeeze layer feature maps divided by the number of Expand layer feature maps is known as the Squeeze ratio, and it is a crucial hyperparameter of the Fire module.The most important part of MobileNetV2 is its depth-wise separable convolution (DWSC) layer, which gives it its extraordinary speed.Pointwise convolution (PWC) and Depthwise convolution (DWC) are the two stages in depthwise separable convolution (DWSC). DWC operations, as opposed to standard convolution, which operates on all M channels concurrently, only apply convolution to one channel at a time. 1×1 convolution is applied to the M channels in the pointwise operation. In this process, a $1 \times 1 \times M$ filter will be used.

4. Result and Discussion

In this section, the lung cancer detection using the proposed model is evaluated using the performance metrics like accuracy, sensitivity, specificity, precision, recall, F-Measure, NPV (Negative predictive value) , FPR (False positive ratio) , FNR (False negative ratio) and MCC (Matthews correlation coefficient) . The lung cancer prediction dataset [26] is used for evaluation. In this dataset, the total data is divided into training (70%), testing (20%) and validation (10%). The implementation is performed in the MATLAB platform.Table 1 presents a comprehensive comparison of performance metrics between the proposed lung cancer detection method and existing methods such as MobileNetV2, ResNet101, SqueezeNet, AlexNet, and DarkNet.

Table 1. Comparison of performance metrics with the proposed and existing method

Metric	Proposed	Mobile NetV2	ResNet101	SqueezeNet	AlexNet	DarkNet
Sensitivity	0.973	0.96	0.937	0.835	0.781	0.772
Specificity	0.999	0.994	0.989	0.94	0.93	0.935
Accuracy	0.988	0.987	0.962	0.923	0.911	0.903
Precision	0.971	0.964	0.949	0.842	0.788	0.77
Recall	0.986	0.951	0.927	0.828	0.798	0.775
FMeasure	0.971	0.966	0.948	0.832	0.807	0.775
NPV	0.995	0.995	0.99	0.97	0.95	0.939
FPR	0.024	0.032	0.03	0.075	0.089	0.105
FNR	0.067	0.07	0.087	0.198	0.252	0.27
MCC	0.954	0.925	0.901	0.779	0.717	0.695

The proposed method performs better on a variety of metrics compared to the other models. The high sensitivity of 0.973 indicates its effectiveness in identifying genuine positive cases of lung cancer. The robust ability to correctly identify true negative cases is indicated by the exceptionally high specificity of 0.999. The proposed method is considered reliable in correctly predicting both positive and negative instances, as indicated by the overall high accuracy of 0.988.The proposed approach also performs well in terms of recall of 0.986, F- measure of 0.971, and NPV of 0.995, all of which together show that it balances capturing positive instances with preventing false positives. The model can reduce errors, as demonstrated by the low FNR of 0.067 and FPR of 0.024.The proposed model exhibits strong overall performance, as indicated by the MCC of 0.954, which provides a comprehensive evaluation. Comparatively, the proposed approach consistently outperforms existing methods, despite their generally acceptable results.

4.1. Performance analysis

Figure 4 to 8 shows the graphical analysis of the various performance metrics with the existing methods like MobileNetV2, ResNet101, SqueezeNet, AlexNet, and DarkNet.

Figure 4 illustrates the performance analysis of sensitivity and specificity with the proposed and the existing methods.

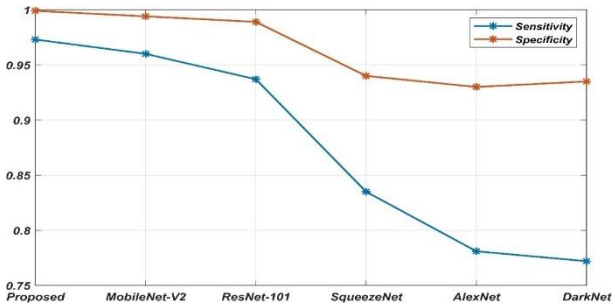

Figure 4: Analysis of sensitivity and specificity

The proposed detection model acquires a strong sensitivity score of 0.973, suggesting a reliable ability to identify positive cases of lung cancer. This outperforms the individual sensitivity scores of MobileNetV2 of 0.96, ResNet101 of 0.937, SqueezeNet of 0.835, AlexNet of 0.781, and DarkNet of 0.772. Among the models that were compared, the proposed model stands out as having the highest sensitivity, highlighting its efficacy in identifying cases of lung cancer.The proposed FuzSquResMobileNet model exhibits a very high 0.999 specificity. This suggests that the model performs exceptionally well at correctly ruling out negative cases, which helps to reduce the number of false positives in the detection of lung cancer. When compared to the suggested model, MobileNetV2, ResNet101, and SqueezeNet show specificities of 0.994, 0.989, and 0.94, respectively.

The performance analysis of accuracy andprecision fortheproposed and the current methods is shown in Figure 5.

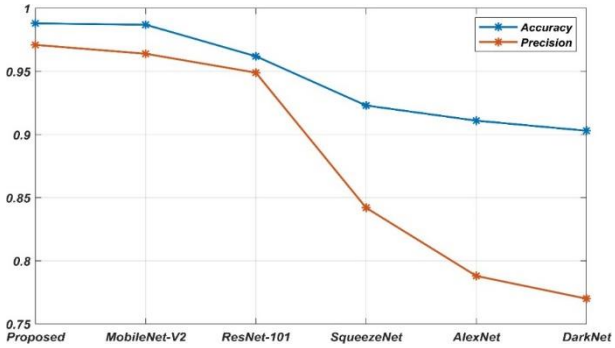

Figure 5: Analysis of accuracy and precision

The proposed model with an accuracy of 0.988, shows that it is very good at correctly predicting both positive and negative cases in the detection of lung cancer. Additionally, MobileNetV2, ResNet101, and SqueezeNet demonstrate strong accuracies of 0.987, 0.962, and 0.923, respectively, demonstrating their general dependability in producing accurate predictions. Among the models compared, the proposed model stands out with the highest accuracy, highlighting its efficacy in offering accurate and reliable predictions for lung cancer detection. The proposed model has a precision of 0.971, demonstrating its ability to detect lung cancer with a high degree of accuracy and positive predictions. SqueezeNet, ResNet101, and MobileNetV2 also exhibit the precision values of 0.842, 0.949, and 0.964, respectively, demonstrating their efficacy in reducing false positives.

The Recall and NPV performance analysis for theproposed and the existing methods is shown in Figure 6.

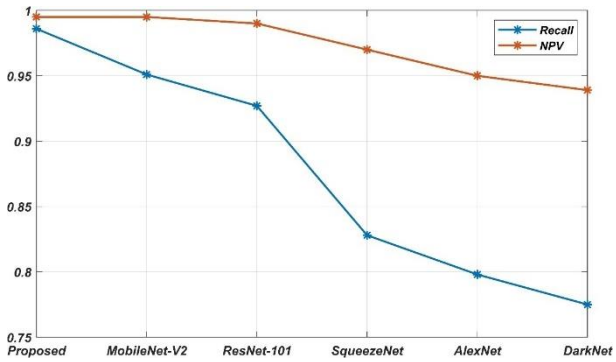

Figure 6: Analysis of Recall and NPV

The proposed model has a high recall of 0.986, which highlights its remarkable ability to accurately identify almost 99% of real positive cases of lung cancer. In contrast, MobileNetV2, ResNet101, and SqueezeNet all show the recalls of 0.951, 0.927, and 0.828, respectively, indicating that they can recognize positive instances, though at slightly lower rates than the proposed framework. The proposed model has an exceptionally high NPV of 0.995, which suggests that it is accurate in predicting negative cases. Additionally, MobileNetV2, ResNet101, and SqueezeNet demonstrate a high NPV of 0.995, 0.99, and 0.97, respectively, demonstrating their accuracy in excluding negative instances. Conventional models like DarkNet and AlexNet also show acceptable NPVs of 0.939 and 0.95, respectively.

Figure 7 illustrates the performance analysis of F-measure and MCC with the proposed and the existing methods.

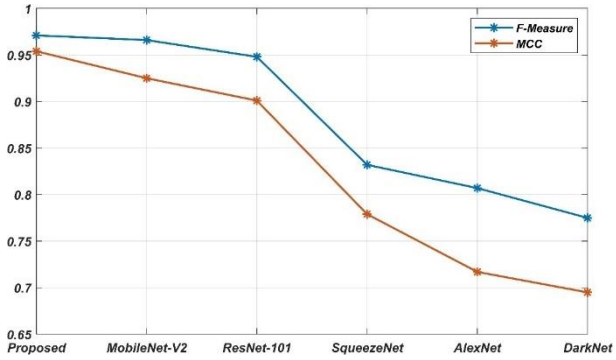

Figure 7: Analysis of F-measure and MCC

The proposed model with the highest F-measure of 0.971 exhibits an acceptable balance between precision and recall. This implies that the model performs well in both recalling actual positive instances and accurately predicting positive outcomes. F-measure of 0.966, 0.948, and 0.832, respectively, are also displayed by MobileNetV2, ResNet101, and SqueezeNet, demonstrating their overall efficacy in striking a balance between recall and precision. Conventional models like AlexNet and DarkNet exhibit a relatively lower F-measure of 0.807 and 0.775, respectively. MobileNetV2, ResNet101, and SqueezeNet also display respectable MCC values of 0.901, 0.779, and 0.925, respectively. The proposed model performs well overall in the detection of lung cancer with a high MCC of 0.954. This implies that the model successfully manages the trade-off between false positives and false negatives in addition to having high sensitivity and specificity. The proposed model has the

highest MCC, indicating its capacity to offer a thorough and impartial evaluation of its performance in lung cancer detection.

The performance analysis of FPR and FNR fortheproposed and current methods is shown in Figure 8.

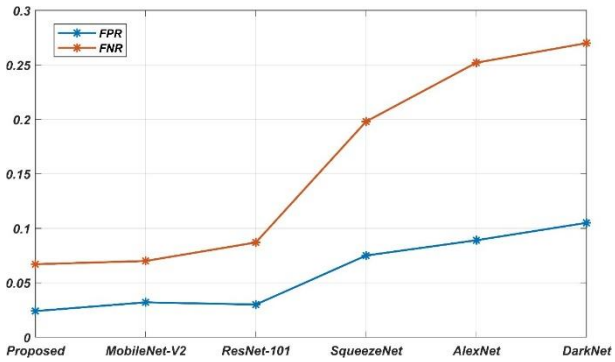

Figure 8: Analysis of FPR and FNR

The proposed model with a low FPR of 0.024, shows that only a small percentage of real negative instances are mistakenly identified as positive. A low false positive rate (FPR) is preferable in medical applications because it suggests a reduced chance of false alarms or needless treatments for patients who do not have lung cancer. SqueezeNet, MobileNetV2, and ResNet101 display comparatively low FPR values of 0.032, 0.03, and 0.075, respectively, demonstrating their efficacy in preventing false positives. The proposed model's FNR of 0.067 indicates a comparatively low rate of false negatives. This suggests that the model has a high sensitivity for detecting lung cancer because it accounts for a sizable fraction of positive cases. Compared to the other models, the proposed model achieved the lowest error rate achieving the precise detection of lung cancer.

5. Conclusion

This research presented a novel techniqueto detectthelung cancer, addressing the urgent need for early diagnosis to raise global survival rates against this deadly and pervasive illness. The Mask R-CNN can be precisely identified as the Region of Interest through the combination of the Modified Fuzzy Analytic Hierarchy Process and a hybrid ChimpGaz optimization algorithm. This process guarantees the best possible parameter configurations. The hybrid optimization algorithm augments the discriminatory power of the feature ranking system by employing a Modified Fuzzy AHP with sigmoid membership functions. The proposed model, "FuzSquResMobileNet," combines fuzzy logic-based preliminary detection with pre-trained deep learning models (SqueezeNet, ResNet101, and MobileNetv2). This combination yields a thorough method of feature extraction, which raises detection accuracy overall. The evaluation metrics demonstrate the validity of the suggested approach, with a high accuracy of 0.988 demonstrating a potent ability to accurately predict both positive and negative events. Low FNR and FPR values emphasize how well the model can reduce errors, which further supports its dependability. The MCC of 0.954 indicates the overall performance, which shows how reliable the proposed approach is at offering a thorough assessment. The new method continuously outperforms current methods, which is significant because it highlights the potential of this approach as a useful tool for lung cancer detection. The outcome of this work represents a major advancement in the development of more precise and trustworthy diagnostic tools, which will ultimately lead to better patient outcomes and care in the fight against lung cancer.

References

[1] Asuntha, A. and Srinivasan, A., 2020. Deep learning for lung Cancer detection and classification. *Multimedia Tools and Applications*, *79*, pp.7731-7762.

[2] Bray, F., Ferlay, J., Soerjomataram, I., Siegel, R.L., Torre, L.A. and Jemal, A., 2018. Global cancer statistics 2018: GLOBOCAN estimates of incidence and mortality worldwide for 36 cancers in 185 countries. *CA: a cancer journal for clinicians*, *68*(6), pp.394-424.

[3] Zhang, C., Sun, X., Dang, K., Li, K., Guo, X.W., Chang, J., Yu, Z.Q., Huang, F.Y., Wu, Y.S., Liang, Z. and Liu, Z.Y., 2019. Toward an expert level of lung cancer detection and classification using a deep convolutional neural network. *The oncologist*, *24*(9), pp.1159-1165.

[4] Günaydin, Ö., Günay, M. and Şengel, Ö., 2019, April. Comparison of lung cancer detection algorithms. In *2019 Scientific Meeting on Electrical-Electronics & Biomedical Engineering and Computer Science (EBBT)* (pp. 1-4). IEEE.

[5] Manoharan, D.S. and Sathesh, A., 2020. Early diagnosis of lung cancer with probability of malignancy calculation and automatic segmentation of lung CT scan images. *Journal of Innovative Image processing*, *2*(4), pp.175-186.

[6] Vas, M. and Dessai, A., 2017, August. Lung cancer detection system using lung CT image processing. In *2017 International Conference on Computing, Communication, Control and Automation (ICCUBEA)* (pp. 1-5). IEEE.

[7] Ohno, Y., Yoshikawa, T., Takenaka, D., Koyama, H., Aoyagi, K., Yui, M., Oshima, Y., Hamabuchi, N., Tanaka, Y., Shigemura, C. and Oota, S., 2022. Small cell lung cancer staging: prospective comparison of conventional staging tests, FDG PET/CT, whole-body MRI, and coregistered FDG PET/MRI. *American Journal of Roentgenology*, *218*(5), pp.899-908.

[8] Akter, O., Moni, M.A., Islam, M.M., Quinn, J.M. and Kamal, A.H.M., 2021. Lung cancer detection using enhanced segmentation accuracy. *Applied Intelligence*, *51*, pp.3391-3404.

[9] Ahmed, U., Rasool, G., Zafar, S. and Maqbool, H.F., 2018, November. Fuzzy rule based diagnostic system to detect the lung cancer. In *2018 International Conference on Computing, Electronic and Electrical Engineering (ICE Cube)* (pp. 1-6). IEEE.

[10] Yamunadevi, M.M. and Ranjani, S.S., 2021. Efficient segmentation of the lung carcinoma by adaptive fuzzy–GLCM (AF-GLCM) with deep learning based classification. *Journal of Ambient Intelligence and Humanized Computing*, *12*, pp.4715-4725.

[11] Asuntha, A. and Srinivasan, A., 2020. Deep learning for lung Cancer detection and classification. *Multimedia Tools and Applications*, *79*, pp.7731-7762.

[12] Jasmine Pemeena Priyadarsini, M., Rajini, G.K., Hariharan, K., Utkarsh Raj, K., Bhargav Ram, K., Indragandhi, V., Subramaniyaswamy, V. and Pandya, S., 2023. Lung Diseases Detection Using Various Deep Learning Algorithms. *Journal of healthcare engineering*, *2023*.

[13] Dafni Rose, J., Jaspin, K. and Vijayakumar, K., 2021. Lung cancer diagnosis based on image fusion and prediction using CT and PET image. *Signal and Image Processing Techniques for the Development of Intelligent Healthcare Systems*, pp.67-86.

[14] Banerjee, N. and Das, S., 2020, March. Prediction lung cancer–in machine learning perspective. In *2020 International Conference on Computer Science, Engineering and Applications (ICCSEA)* (pp. 1-5). IEEE.

[15] Farahani, F.V., Zarandi, M.F. and Ahmadi, A., 2015, August. Fuzzy rule based expert system for diagnosis of lung cancer. In 2015 Annual Conference of the North American Fuzzy Information Processing Society (NAFIPS) held jointly with 2015 5th World Conference on Soft Computing (WConSC) (pp. 1-6). IEEE.

[16] Khalil, A.M., Li, S.G., Lin, Y., Li, H.X. and Ma, S.G., 2020. A new expert system in prediction of lung cancer disease based on fuzzy soft sets. *Soft Computing*, *24*(18), pp.14179-14207.

[17] Palani, D. and Venkatalakshmi, K., 2019. An IoT based predictive modelling for predicting lung cancer using fuzzy cluster based segmentation and classification. *Journal of medical systems*, *43*, pp.1-12.

[18] Hatuwal, B.K. and Thapa, H.C., 2020. Lung cancer detection using convolutional neural network on histopathological images. *Int. J. Comput. Trends Technol*, *68*(10), pp.21-24.

[19] Mishra, S., Thakkar, H.K., Mallick, P.K., Tiwari, P. and Alamri, A., 2021. A sustainable IoHT based computationally intelligent healthcare monitoring system for lung cancer risk detection. *Sustainable Cities and Society*, *72*, p.103079.

[20] Jalaldeen, K., Malathi, M., Sinthia, P., Vadivel, M. and Shankar, B.M., 2021. An automatic identification of lung tumor by using CNN network and fuzzy-clustering algorithm. *Materials Today: Proceedings*, *45*, pp.2921-2924.

[21] Prasad, J., Chakravarty, S. and Krishna, M.V., 2022. Lung cancer detection using an integration of fuzzy K-means clustering and deep learning techniques for CT lung images. *Bulletin of the Polish Academy of Sciences: Technical Sciences*, pp.e139006-e139006.

[22] Tiwari, L., Raja, R., Awasthi, V., Miri, R., Sinha, G.R., Alkinani, M.H. and Polat, K., 2021. Detection of lung nodule and cancer using novel Mask-3 FCM and TWEDLNN algorithms. *Measurement*, *172*, p.108882.

[23] Lakshmanaprabu, S.K., Mohanty, S.N., Shankar, K., Arunkumar, N. and Ramirez, G., 2019. Optimal deep learning model for classification of lung cancer on CT images. *Future Generation Computer Systems*, *92*, pp.374-382.

[24] Hussain, L., Aziz, W., Alshdadi, A.A., Nadeem, M.S.A. and Khan, I.R., 2019. Analyzing the dynamics of lung cancer imaging data using refined fuzzy entropy methods by extracting different features. *IEEE Access*, *7*, pp.64704-64721.

[25] Masood, A., Sheng, B., Yang, P., Li, P., Li, H., Kim, J. and Feng, D.D., 2020. Automated decision support system for lung cancer detection and classification via enhanced RFCN with multilayer fusion RPN. *IEEE Transactions on Industrial Informatics*, *16*(12), pp.7791-7801.

[26] Dataset is taken from https://www.kaggle.com/datasets/thedevastator/cancer-patients-and-air-pollution-a-new-link.